P H Y S I C A L   R E V I E W   L E T T E R S

Caustics due to a Negative Refractive Index in Circular Graphene *p-n* Junctions

József Cserti, András Pályi, and Csaba Péterfalvi

Department of Physics of Complex Systems, Eötvös University, H-1117 Budapest, Pázmány Péter sétány 1/A, Hungary
(Received 27 June 2007; published 11 December 2007)

We show that the wave functions form caustics in circular graphene *p-n* junctions which in the framework of geometrical optics can be interpreted with a negative refractive index.

The possibility of a negative refractive index in nature was first analyzed theoretically by Veselago [1] and was followed by other important works [2]. Evidence for such left-handed metamaterials has been demonstrated by microwave experiments [3].

Another prominent candidate for such materials might be graphene, as proposed recently by Cheianov *et al.* [4]. They studied the transmission of electrons through a plane *p-n* junction of graphene and showed that the optics of electron flow, in the framework of geometrical optics, can be described by optical refraction with negative refractive index. The graphene itself provides many other peculiar electronic properties owing to the close similarity between the dispersion relation of two-dimensional massless Dirac fermions and the low energy electronic spectrum of graphene (for a review, see [5]). However, an easy way of tuning the refractive index by gate potential may open up further research directions in graphene physics. For example, graphene might be utilized to fabricate properly designed electronic lens.

One of the interesting subjects in geometrical optics is the caustics. A caustic is an envelope of a family of rays at which the density of rays is singular. The caustics have been extensively studied in the past (for a review see, e.g., the work by Berry and Upstill [6]). As in Ref. [4] for plane *p-n* junction, we show theoretically that in circular *p-n* junction of graphene the caustics can also arise in the wave function pattern of electrons, and the curves of caustics can be calculated using the well-known Snell's law with negative refractive index.

To this end, we consider the scattering of ballistic incident electrons in graphene shown in Fig. 1. To demonstrate the formation of caustics in circular *p-n* junctions, we used a simple gate potential $V(r) = V_0 \Theta(R - r)$, where Θ denotes the Heaviside function. The assumption of such a sharp potential is valid provided that $\lambda_F \gg d$, where λ_F is the Fermi wavelength outside the junction and d is the characteristic length scale in which the scattering potential varies. Moreover, to prevent intervalley scattering it is necessary that $d \gg a$, where a is the lattice constant of graphene [4,7]. The negative refractive index is realized by *p-n* junctions of graphene in which the energy E of the incoming electrons at the *n* side is positive (belonging to the conduction band), while at the *p* side of the junction the potential V_0 is chosen such that $E < V_0$; therefore, the

electrons belong to the valence band. Here we focus on this case ($0 < E < V_0$) but its generalization to arbitrary values of E is straightforward. Note that various properties of elastic electron scattering in graphene has already been studied [8]. Here we investigate the wave function pattern inside the junction. Pronounced formation of the caustics can only be seen in the quasiclassical limit, i.e., in case of $R \gg \lambda_F$, but no such condition is assumed in our exact calculation of the wave functions.

The Hamiltonian for the above described scattering problem for energies E close to the Dirac point may be written as

$$H = H_0 + V(\mathbf{r})\mathbb{1} = c\boldsymbol{\sigma} \cdot \mathbf{p} + V(\mathbf{r})\mathbb{1}. \qquad (1)$$

Here c is the Fermi velocity, $\mathbf{p} = -i\hbar\partial/\partial\mathbf{r}$, while $\boldsymbol{\sigma} = (\sigma_x, \sigma_y)$ and $\mathbb{1}$ are the Pauli matrices and the unit matrix acting in isospin space.

Consider the elastic scattering of incoming electrons governed by the Hamiltonian H. The scattering of the incident electron can be calculated by the generalization of the well-known partial wave method (see, e.g., [9]). The wave function (in polar coordinates) describing the scattering of a single incoming partial wave $h_j^{(2)}$ (defined below) outside the scattering region ($r > R$) can be written in terms of the cylindrical wave eigenfunctions of the Hamiltonian H with energy $E > 0$:

$$\Psi_j^{(\text{out})} = h_j^{(2)} + S_j h_j^{(1)}, \qquad (2a)$$

where

$$h_j^{(d)}(r, \varphi) = \begin{pmatrix} H_{j-(1/2)}^{(d)}(k_{\text{out}}r)e^{-i\varphi/2} \\ iH_{j+(1/2)}^{(d)}(k_{\text{out}}r)e^{i\varphi/2} \end{pmatrix} e^{ij\varphi}, \qquad (2b)$$
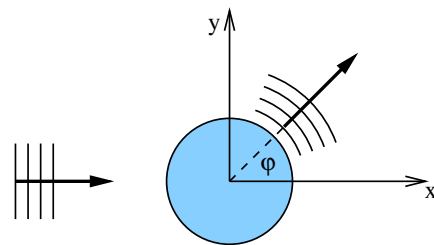

FIG. 1 (color online).   Incident plane wave of electron in single layer graphene is scattered by a rotational symmetric potential $V(r)$ (circular region).

while inside the scattering region ($r < R$) the wave function reads

$$\Psi_j^{(in)} = A_j \chi_j, \tag{3a}$$

where

$$\chi_j(r, \varphi) = \begin{pmatrix} J_{j-(1/2)}(k_{in}r)e^{-i\varphi/2} \\ -iJ_{j+(1/2)}(k_{in}r)e^{i\varphi/2} \end{pmatrix} e^{ij\varphi}. \tag{3b}$$

Here the pseudo-angular momentum $j \in \mathbb{J} \equiv \{\ldots, -\frac{3}{2}, -\frac{1}{2}, \frac{1}{2}, \frac{3}{2}, \ldots\}$, $h_j^{(1)}$ ($h_j^{(2)}$) is an outgoing (incoming) cylindrical wave function corresponding to $d = 1$ ($d = 2$). The wave numbers are $k_{out} = E/(\hbar c) > 0$ and $k_{in} = |E - V_0|/(\hbar c) > 0$, while J_n refers to the Bessel function of the first kind, and $H_n^{(1)}$ and $H_n^{(2)}$ are the Hankel functions of the first and second kind, respectively [10]. To construct the eigenfunctions we used the fact that for rotational symmetric potential $[J_z, H] = 0$ holds, where $J_z = -i\hbar\partial_\varphi + \hbar\sigma_z/2$ is the pseudo-angular momentum operator. Therefore, the pseudo-angular momentum is a conserved quantity in the scattering process.

The scattering matrix S_j and the amplitude A_j are determined from the boundary conditions, i.e., from the continuity of the total wave function at the boundary of the junction: $\Psi_j^{(out)}(r = R, \varphi) = \Psi_j^{(in)}(r = R, \varphi)$. Then, it is easy to find that

$$S_j = \frac{-H_{j-(1/2)}^{(2)}(X)J_{j+(1/2)}(X') - H_{j+(1/2)}^{(2)}(X)J_{j-(1/2)}(X')}{D_j}, \tag{4a}$$

$$A_j = \frac{H_{j-(1/2)}^{(2)}(X)H_{j+(1/2)}^{(1)}(X) - H_{j+(1/2)}^{(2)}(X)H_{j-(1/2)}^{(1)}(X)}{D_j}, \tag{4b}$$

$$D_j = H_{j+(1/2)}^{(1)}(X)J_{j-(1/2)}(X') + H_{j-(1/2)}^{(1)}(X)J_{j+(1/2)}(X'), \tag{4c}$$

where $X = k_{out}R$ and $X' = k_{in}R$.

We now consider the scattering of an incident plane wave of electron in graphene for $r > R$. Such an eigenstate with energy E has the form

$$\Phi_{\varphi_i}(r, \varphi) = \eta(\varphi_i)e^{ik_{out}r\cos(\varphi-\varphi_i)}, \tag{5a}$$

where

$$\eta(\varphi_i) = \frac{1}{\sqrt{2}}\begin{pmatrix} e^{-i\varphi_i/2} \\ e^{i\varphi_i/2} \end{pmatrix} \tag{5b}$$

and φ_i denotes the direction of the propagation of the incident electron. Using the properties of the Hankel functions [10] one can show that the partial wave expansion of Φ_{φ_i} is

$$\Phi_{\varphi_i} = \frac{1}{2}\sum_{j\in\mathbb{J}} i^{j-(1/2)}(h_j^{(2)} + h_j^{(1)})e^{-ij\varphi_i}. \tag{6}$$

Without the loss of generalization, we choose the direction of propagation to be parallel with the x axis, which means $\varphi_i = 0$ in (5a). Then the wave function for $r > R$ is given by

$$\Psi^{(out)} = \Phi_{\varphi_i=0} + \frac{1}{2}\sum_{j\in\mathbb{J}} i^{j-(1/2)}(S_j - 1)h_j^{(1)}, \tag{7a}$$

and the wave function for $r < R$ is given by

$$\Psi^{(in)} = \frac{1}{2}\sum_{j\in\mathbb{J}} i^{j-(1/2)}A_j\chi_j. \tag{7b}$$

Note that the second term in (7a) is the scattered wave due to the scattering of the incident plane wave Φ_{φ_i} on the scattering region described by the potential $V(r) = V_0\Theta(R - r)$. The scattering cross section can be obtained from the asymptotic form ($r \gg R$) of the scattered wave.

Equations (4) and (7) allows us to calculate exactly the wave functions both inside and outside the junction. Note that the wave functions depend only on the two dimensionless parameters, $k_{in}R$ and $k_{out}R$. Figures 2 and 3 show how the incident plane wave (from direction $\varphi_i = 0$) penetrates into the circular region of the p-n junction. For $r < R$, the formation of the caustics in the wave function patterns is clearly visible along the solid and dotted lines. Vodo et al. found a similar wave pattern experimentally by focusing a plane microwave with a plano-concave lens fabricated from a photonic crystal having negative refractive index [11].

In a sharp p-n junction of graphene the optics of electron flow [4] is very much the same as in photonic crystals with negative refractive index. In a similar way as in Ref. [4] for our circular p-n junction the Snell's law reads
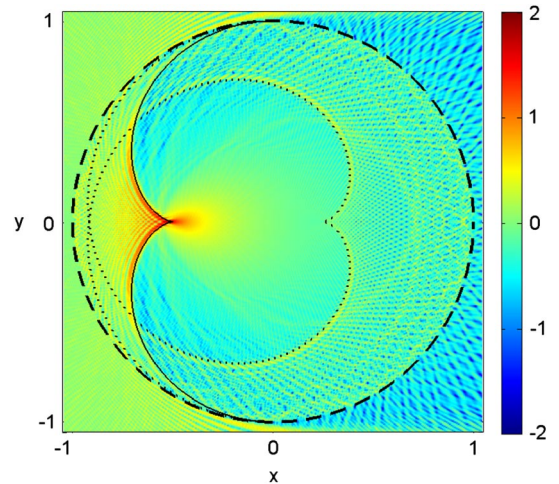

FIG. 2 (color online). $|\Psi|^2$ (in scale of logarithmic to base 10) is plotted inside and outside, close to the scattering region (the dashed line shows the boundary of the p-n junction). Here $k_{in}R = 300$ and $k_{out}R = 300$ corresponding to $n = -1$, and x and y are in units of R. The solid (dotted) line corresponds to the caustic for $p = 1$ ($p = 2$) (see the text).
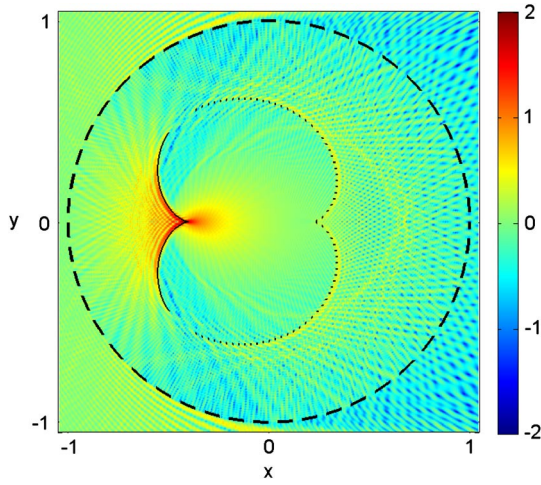
FIG. 3 (color online).   The same as in Fig. 2 with $k_{in}R = 300$ and $k_{out}R = 200$ corresponding to $n = -1.5$.

$$\frac{\sin\alpha}{\sin\beta} = n = -\frac{k_{in}}{k_{out}}, \tag{8}$$

where α and β are the angle of incidence and refraction, respectively. Since in our calculation both k_{in} and k_{out} are positive the refractive index becomes negative similarly as for properly designed photonic crystals.

In what follows we show that the intensity maximum in the wave function patterns is around the caustic and can be understood by the Snell's law (8) with negative refractive index. Figure 4 shows how the incident ray refracts at the boundary of the circular p-n junction and then after $p - 1$ internal reflections exits from the junction. One can classify the different ray paths by the impact parameter $b = R \sin\alpha$ and the number of chords p inside the circle corresponding to $p - 1$ internal reflections. Incident rays with varying impact parameters ($-R \leq b \leq R$) form a family of rays inside the circle. The envelope of this ray family results in a caustic as shown in Fig. 5. Each of the chords has its own caustic.

Using differential geometry to calculate the envelope of family of curves we find that the curve $\mathbf{r}_c$ (in Descartes coordinates shown in Fig. 4) of the caustic of the pth chord is given by

$$\frac{\mathbf{r}_c(p, \alpha)}{R} = (-1)^{p-1}\left[\begin{pmatrix} -\cos\Theta \\ \sin\Theta \end{pmatrix} + \cos\beta \frac{1 + 2(p-1)\beta'}{1 + (2p-1)\beta'}\right.$$
$$\left.\times \begin{pmatrix} \cos(\Theta + \beta) \\ -\sin(\Theta + \beta) \end{pmatrix}\right], \tag{9a}$$

$$\Theta(p, \alpha) = \alpha + 2(p-1)\beta, \tag{9b}$$

$$\sin\beta = \frac{\sin\alpha}{|n|}, \tag{9c}$$

$$\beta' = \frac{\cos\alpha}{\sqrt{n^2 - \sin^2\alpha}}. \tag{9d}$$

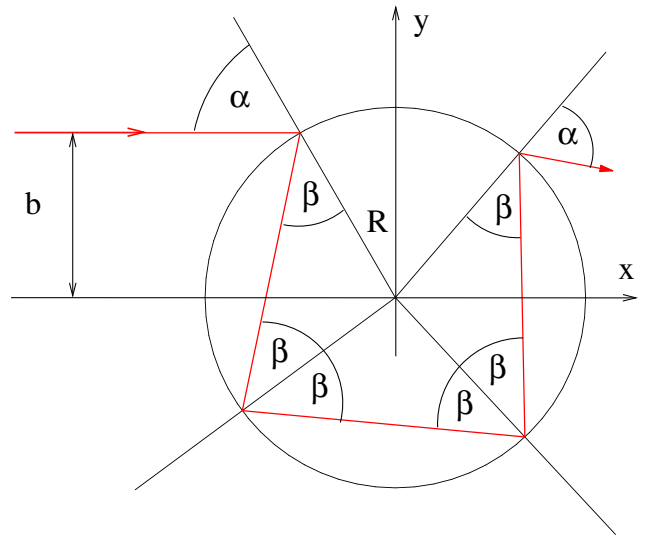Here α varies between $-\pi/2$ and $\pi/2$ and the prime

FIG. 4 (color online).   The basic geometry of ray paths inside the circular p-n junction. The incident ray from left with impact parameter b and angle of incidence α is refracted at the boundary of the junction with angle β and then after $p - 1$ internal reflections exits from the junction. Here $p = 3$ and we set $n = -1.3$ and $\alpha = 60°$.

denotes the derivation with respect to α. This is a parametric curve for caustics with parameter α. Figures 2 and 3 show the caustics calculated from Eq. (9). In both cases, one can see that the location of the caustics formed from the interference pattern of the exact wave functions inside the junction agrees very well with that obtained from Snell's law with negative refractive index. The caustics for $p > 2$ are less visible since after each internal reflection the intensity of the rays decreases.

It is clear from Eq. (9) that for a given p the caustics are completely determined by the value of the refractive index n. The caustics in a circular p-n junction belong to the class of cusp according to the catastrophe optics [6]. As a consequence of the reflection symmetry of the system with respect to the x axis, the caustics show this symmetry as well. This implies that the cusps are always located on the x axis. The location of the cusp $(x, y) = (x_{cusp}, 0)$ (in polar coordinates) for the pth chord can be obtained from (9) by setting $\alpha = 0$ and we find

$$x_{cusp}(p) = \frac{(-1)^p}{|n| - 1 + 2p}R. \tag{10}$$

The cusps show "alternating" features in two respects. First, the sign of the coordinate x_{cusp} is determined by the parity of p, and the position of the cusp gradually approaches the origin with increasing p. Second, the orientation of the cusp, i.e., if it points towards the positive or negative x direction, is also determined by the parity of p.

As can be seen in Fig. 5 the paraxial ($\alpha \ll 1$) incident rays entering into the circular region of the graphene junction are focused at the focal point for $p = 1$. The focal length f measured from the point $(r, \varphi) = (R, \pi)$ is given
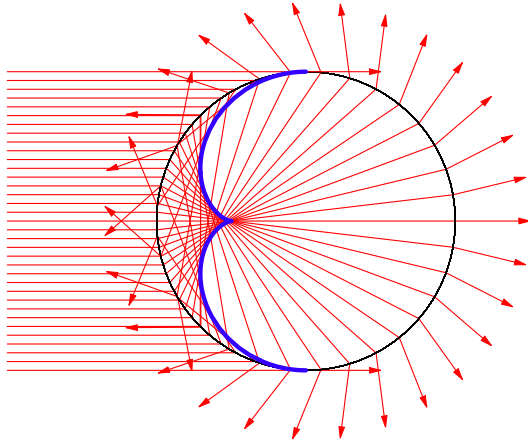
FIG. 5 (color online). Caustic inside the *p-n* junction formed from the envelope of the refracted ray paths of different incident rays. The thick solid line is the caustic curve calculated from (9). Here $p = 1$ and $n = -1$.

by the location of the cusp: $f = R - |x_{cusp}| = R|n|/(|n| + 1)$. The same is obtained when the refractive index is replaced by its negative value in the expression of the image focal length defined in ordinary geometrical optics [12]. To demonstrate the negative refractive index in the photonic crystal experiment [11] the focal length was measured.

To realize the predicted caustic formation and focusing effect in an experiment, one needs to collimate a mono-directional electron beam onto the circular scattering region. This might be achieved utilizing a *smooth planar p-n junction* which is known to transmit only those quasiparticles that approach it almost perpendicular to the *p-n* interface [13]. Therefore, a possible experimental setup could be built up from a source electrode, a selectively transmitting smooth planar *p-n* junction, the circular scattering region, and a drain electrode. Under bias, the spatial dependence of the charge density of the transported electrons might be measured by scanning probe techniques.

Circular *p-n* junctions together with planar ones studied earlier [4] can be a building block of electron optics in graphene. However, the refractive index varies with energy of the incoming electrons; therefore, the temperature needs to be low enough for sharp images. As it is mentioned in the introduction, one needs experimentally that $a \ll d \ll \lambda_F \equiv 2\pi/k_{out}$ (for sharp potential barrier and absence of intervalley scattering). Another condition required to observe sharp interference patterns around the caustics is $k_{in}R \gg 1$ corresponding to the quasiclassical limit. For example, setting $E = 40$ meV, and $V_0 = 80$ meV (using gate potential), $R = 800$ nm, all of these conditions are fulfilled since $d \sim 10$ nm [14], implying that the refractive index is $n = -1$, while $k_{in}R = 50$ and $\lambda_F = 10d$.

In summary, we calculated inside and outside a circular *p-n* junction of graphene the scattered wave function of an incoming plane wave of electrons due to a circular symmetric steplike potential. We showed that the scattered wave function inside the junction has an interference pattern with high intensity maximum located around the caustics calculated from Snell's law with negative refractive index.

[1] V. G. Veselago, Sov. Phys. Usp. **10**, 509 (1968).
[2] J. B. Pendry, Phys. Rev. Lett. **85**, 3966 (2000); Nature (London) **423**, 22 (2003); D. R. Smith, J. B. Pendry, and M. C. K. Wiltshire, Science **305**, 788 (2004).
[3] R. A. Shelby, D. R. Smith, and S. Schultz, Science **292**, 77 (2001); A. A. Houck, J. B. Brock, and I. L. Chuang, Phys. Rev. Lett. **90**, 137401 (2003); C. G. Parazzoli, R. B. Greegor, K. Li, B. E. C. Koltenbah, and M. Tanielian, Phys. Rev. Lett. **90**, 107401 (2003); M. Notomi, Phys. Rev. B **62**, 10 696 (2000); C. Luo, S. G. Johnson, J. D. Joannopoulos, and J. B. Pendry, Opt. Express **11**, 746 (2003).
[4] V. V. Cheianov, V. I. Fal'ko, and B. L. Altshuler, Science **315**, 1252 (2007).
[5] M. I. Katsnelson, Mater. Today **10**, 20 (2007); M. I. Katsnelson and K. S. Novoselov, Solid State Commun. **143**, 3 (2007); A. K. Geim and K. S. Novoselov, Nature Mater. **6**, 183 (2007).
[6] M. V. Berry and C. Upstill, in *Progress in Optics*, edited by E. Wolf (North-Holland, Amsterdam, 1980), pp. 257–346.
[7] M. I. Katsnelson, K. S. Novoselov, and A. K. Geim, Nature Phys. **2**, 620 (2006).
[8] D. P. DiVincenzo and E. J. Mele, Phys. Rev. B **29**, 1685 (1984); T. Ando, T. Nakanishi, and R. Saito, J. Phys. Soc. Jpn. **67**, 2857 (1998); M. Hentschel and F. Guinea, Phys. Rev. B **76**, 115407 (2007); M. I. Katsnelson and A. K. Geim, arXiv:0706.2490.
[9] F. Schwabl, *Quantum Mechanics* (Springer-Verlag, Berlin, 1992).
[10] *Handbook of Mathematical Functions*, edited by M. Abramowitz and I. A. Stegun (Dover, New York, 1972).
[11] P. Vodo, P. V. Parini, W. T. Lu, and S. Sridhar, Appl. Phys. Lett. **86**, 201108 (2005).
[12] E. Hecht, *Optics* (Addison-Wesley, Reading, MA, 2002), 4th ed.
[13] V. V. Cheianov and V. I. Fal'ko, Phys. Rev. B **74**, 041403(R) (2006).
[14] B. Huard, J. A. Sulpizio, N. Stander, K. Todd, B. Yang, and D. Goldhaber-Gordon, Phys. Rev. Lett. **98**, 236803 (2007).